Structural investigation of the three-layer system MgO/Fe/GaAs(001) by means of photoelectron spectroscopy and diffraction

D. Handschak,* T. Lühr, F. Schönbohm, S. Döring, C. Keutner, U. Berges, and C. Westphal
Lehrstuhl für Experimentelle Physik I, Technische Universität Dortmund, Otto-Hahn Straße 4, 44221 Dortmund, Germany
and DELTA, Technische Universität Dortmund, Maria-Goeppert-Mayer Straße 2, 44221 Dortmund, Germany
(Received 7 January 2013; published 16 July 2013)

We report a combined high-resolution photoemission (XPS) and photoelectron diffraction (XPD) investigation of the three layer system MgO/Fe/GaAs(001). Each layer is investigated with regard to its structure. The two dimers model of the GaAs (4 × 2) reconstruction was confirmed by XPD patterns. We find the intermediate Fe layer in a crystalline structure. Further, the study clearly shows a well-ordered epitaxial MgO film on Fe. A careful analysis of the interface signals indicates an interdiffusion at the Fe/GaAs interface and partially shifted magnesium layers at the MgO/Fe interface.

DOI: 10.1103/PhysRevB.88.045313 PACS number(s): 61.05.js, 79.60.−i, 73.25.+i, 73.50.Gr

I. INTRODUCTION

Multiple-layer systems with MgO and Fe are widely used in magnetic tunnel junctions (MTJ), which are applied in read heads of hard disk drives. The functional principle is based on the tunnel magnetoresistance (TMR).[1,2] These TMR components consist of two ferromagnets, which are separated by an insulator.[3] In many cases iron and magnesium-oxide are used as the ferromagnetic and insulating material, respectively. The resistivity between the ferromagnetic contacts is strongly dependent on the mutual directions of magnetic orientation of the two ferromagnetic layers.[4] This observation is attributed to spin-depending scattering at the ferromagnet/insulator interface.[5]

TMR components are also of interest in magnetoresistive random access memories (MRAM).[6] This non-volatile data storage technique offers a way of retaining data without permanent energy consumption for the storage mechanism. In the new field of spintronics, layer systems consisting of iron and gallium-arsenide are in the focus of present research.[7,8] A spintronics system consists of a semiconductor-ferromagnetic junction, where a giant-magnetoresistance effect (GMR) arises. As a separating element in these systems a semiconductor layer is placed between two ferromagnetic films.[9,10] The requirements are a spin injection into semiconductor bands with uniform orientation and a good spin transport over a sufficient distance. Both properties are provided by Fe-GaAs systems.[11,12]

The three-layer system MgO/Fe/GaAs allows a combination of the discussed effects for improving the spin injection into the semiconductor for these electrons created by tunneling through an insulating barrier.[13] In particular, the structure of the interface has a strong influence on the efficiency of the TMR and GMR effects.[14–16] In this study the structural properties of both the MgO-Fe and the internal Fe-GaAs interface are reported, as well as the crystalline properties of the GaAs, Fe, and MgO layers.

In order to investigate the structure of each layer XPD was applied. XPD combines core-level photoemission spectroscopy with intensity variations as a function of polar and azimuth angles.[17,18] The intensity variations are a result of diffraction and scattering events of the outgoing electron wave at neighboring atoms around the emitter atom. It is widely used for structural investigations with great success.[19] Additionally, if sufficient spectral resolution is available, high-resolution XPS spectra allow a detailed analysis for each element and its chemical environment. The spectral components contained in the photoemission signals provide information on the local bonding, e.g., whether the emitter is located as a part of a dimer at the surface or located within a bonding beneath the surface.[20] We compare experimental and simulated XPD patterns for various models.

Iron grows crystalline on GaAs(001) if prepared on a (4 × 2)-reconstructed surface as reported by Mossbühler *et al.*[21] This GaAs surface is one of the most gallium-rich surfaces and since the iron interaction to gallium is less favorable than to arsenide it is assumed that the crystalline growth is supported by a rather low adsorbate-surface interaction.[22,23] As a result, the previously proposed structure (from STM images) of the GaAs (4 × 2) reconstruction[24,25] is impressively confirmed by XPD. Up until now it was unclear whether the Fe film undergoes a structural change if MgO is prepared on top of Fe. The crystalline properties of the Fe layer grown on the GaAs (4 × 2) reconstruction and MgO grown on this Fe film are confirmed within the high-resolution XPS and XPD analysis. Furthermore, we find that the Fe/MgO interface consists of oxidized iron and shifted magnesium layers, while the XPS and XPD analyses indicate a mixed Fe/GaAs interface.

II. EXPERIMENTAL SETUP

The measurements were performed in an ultrahigh vacuum chamber with a base pressure of approximately $p = 5 \times 10^{-11}$ mbar at beamline 11 at the storage ring DELTA in Dortmund, Germany. The chamber contains a hemispherical electron analyzer, an electron beam evaporator, a sputter gun, and a low-energy electron diffraction system (LEED). The sample can be moved by a manipulator in all three spatial directions as well as in azimuth- and polar-angle rotations. In this study x-ray energies of $h\nu = 90$ eV and $h\nu = 180$ eV with resulting kinetic energies in the range of $48 < E_{kin} < 129$ eV for the As $3d$, Ga $3d$, Fe $3p$, and Mg $2p$ binding states were

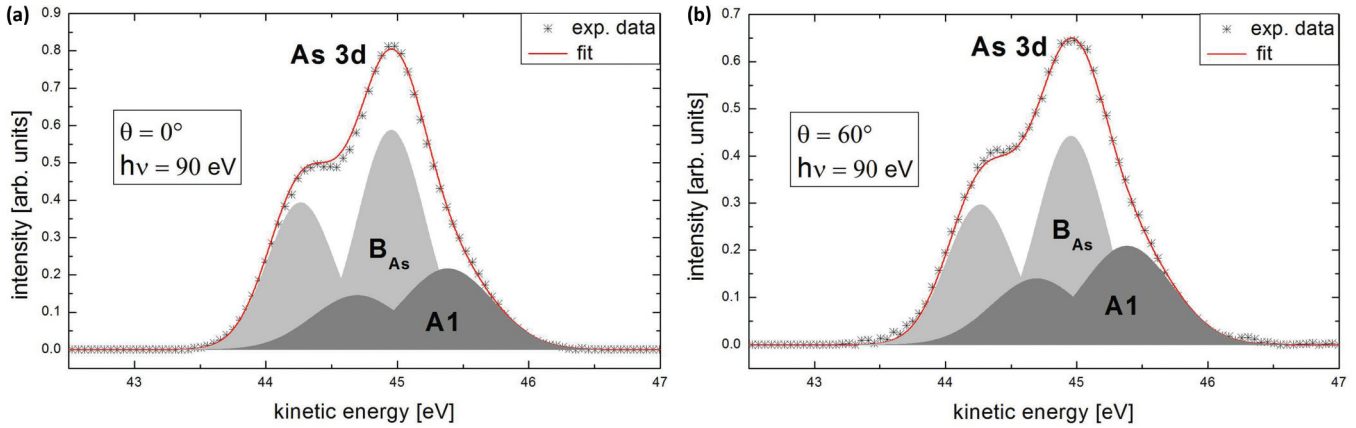

FIG. 1. (Color online) Results of the least-squares fit of As 3*d* spectra of the clean (4 × 2)-reconstructed surface. The spectra are recorded at $\theta = 0^\circ$ (a) and $\theta = 60^\circ$ (b) in order to enhance surface and bulk sensitivity, respectively. The ratio of the bulk component B_{As} to the surface component $A1$ is varying with photoemission direction. The discrepancies between fitted and experimental line shapes could result from keeping a constant branching ratio in the analysis, while a nonstatistical value depending on the emission angle was reported by Bullock *et al.*[38] Those measurements indicated that the angular dependence is a diffraction effect due to the different electron wavelengths of the spin-orbit split components.

used. Each of the individual high-resolution XPS core-level spectra was fitted by using a Gaussian function

$$G(E) = \sum_i \left[A_i \exp\left(\frac{1}{2} \left[\frac{E - E_i}{\sigma_i} \right]^2 \right) + h_{LS}\, A_i \exp\left(\frac{1}{2} \left[\frac{E - (E_i - f_{LS})}{\sigma_i} \right]^2 \right) \right], \quad (1)$$

where A_i denotes the complex amplitude, and σ_i the full width at half maximum (FHWM). The parameters h_{LS} and f_{LS} include the height ratio and the energy shift caused by the spin-orbit coupling (SOC). In all spectra the background was removed by a Shirley function.[26–28] In the following we compare high-resolution spectra recorded at $\theta = 0^\circ$ and $\theta = 60^\circ$ in order to identify the components within a spectrum related to atoms in subsurface and surface regions, respectively.

Within the XPD measurements both polar and azimuth angles were changed, with a polar-angle range of $0^\circ \leqslant \theta \leqslant 60^\circ$ and an azimuth-angle range of $0^\circ \leqslant \phi \leqslant 360^\circ$; the step-width increment was set to $\Delta\theta = 2^\circ$ and $\Delta\phi = 1.8^\circ$. In total this leads to approximately 6000 individual XPS spectra recorded for the hemisphere above the sample. Due to elastic scattering and diffraction effects the intensity of the photoemission signal varies as a function of emission direction.[29] The anisotropy function is defined as $\chi(\theta,\phi) = [I(\theta,\phi) - I_0(\theta)]/I_0(\theta)$, where $I(\theta,\phi)$ and $I_0(\theta)$ denote the intensity at the emission direction (θ,ϕ) and the average intensity at emission direction (θ), respectively.[30,31] For analyzing the experimental XPD patterns we compare these with simulated patterns obtained for various models of the crystal structures. Within the simulations, the full multiple scattering code for low-energy photoelectron diffraction (MSPHD) was applied, which is an excellent tool for structure investigations.[32,33] The atomic cluster size depends on the simulated system; we used 122 atoms for GaAs(4 × 2), and about 50–100 atoms for the Fe bcc and the MgO/Fe system. The angular momentum cutoff for the MSPHD simulations was set up to $l_{max} = 6$. For a quantitative

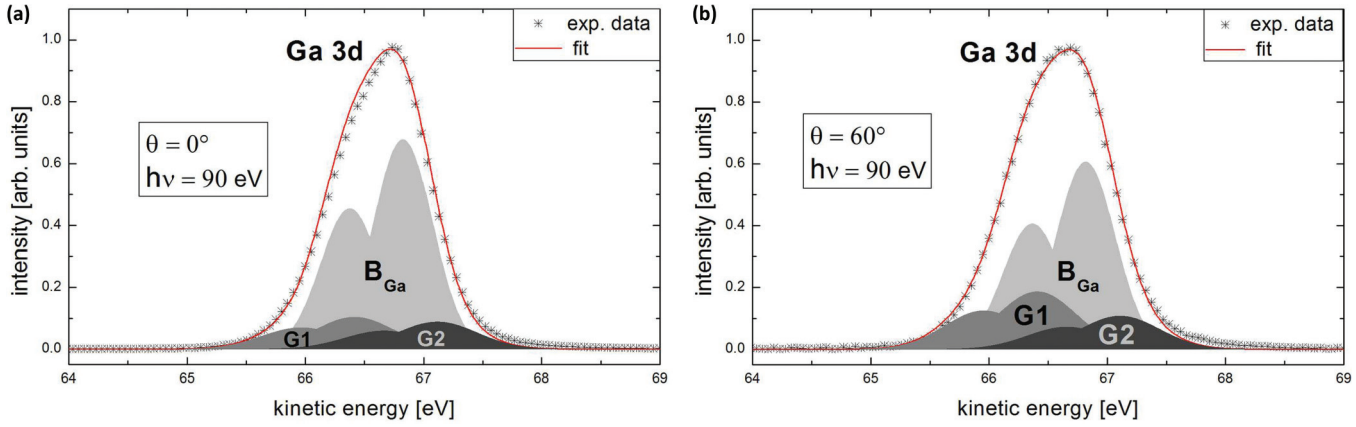

FIG. 2. (Color online) Results of the least-squares fit of Ga 3*d* spectra of the clean (4 × 2)-reconstructed surface. The spectra are recorded at $\theta = 0^\circ$ (a) and $\theta = 60^\circ$ (b) in order to enhance surface and bulk sensitivity, respectively. An intensity change of the bulk component B_{Ga} related to the surface components ($G1$ and $G2$) as well as the intensity variation of $G1$ and $G2$ as a function of polar angle is displayed.

TABLE I. Parameters of the Gaussian fit for the As 3*d* core-level spectra of Fig. 1 and Ga 3*d* spectra of Fig. 2. The intensity ratio of the $3d_{5/2}$ and $3d_{3/2}$ spin-orbit split components was set constant to 4:3.

	E_{kin} (eV)	FHWM (eV)	SOC (eV)
As bulk	44.95	0.25	0.69
*A*1	45.38	0.33	0.69
Ga bulk	66.82	0.24	0.45
*G*1	66.41	0.32	0.45
*G*2	67.13	0.33	0.45

comparison between experimental and simulated diffraction patterns an *R* factor was used, which is defined as

$$R = \frac{\sum_i (\chi_{exp_i} - \chi_{sim_i})^2}{\sum_j \left(\chi^2_{exp_j} - \chi^2_{sim_j}\right)}. \quad (2)$$

In this definition[34] an *R* factor of 2 corresponds to a fully anticorrelated intensity distribution between experimental and simulated XPD patterns. A perfect agreement is indicated by an *R* factor of 0. The simulation had to be performed for a large number of possible atom positions, thus the numerical effort is rather high. Therefore, a genetic algorithm was applied in order to reduce the number of calculations. Genetic algorithms are very suitable tools for minimizing the *R* factor because they avoid local minima and have been widely used with great success.[35]

III. SAMPLE PREPARATION

All samples were cut from a single-crystalline Te-doped GaAs(001) wafer with an orientation better than 0.05°. The sample was prepared by cleaning in acetone in an ultrasonic bath and then transferred to the UHV chamber. In the chamber the sample and the sample holder were heated at $T \approx 600\,^{\circ}\mathrm{C}$ for several hours, terminated by a continuous reduction of the sample's heating current to zero within 5 min.

The surface reconstruction was optimized by repeated argon sputter and annealing cycles. Sputtering was performed with a beam energy of 1000 eV. Annealing was carried out with a temperature increase of $\Delta T = 20\,^{\circ}\mathrm{C/min}$ until $T = 550\,^{\circ}\mathrm{C}$ was reached. This temperature was kept constant for 45 min followed by a temperature reduction to room temperature with the same rate. After this procedure a well-ordered LEED pattern of a (4×2)-reconstructed GaAs(001) surface was observed.

In a next step, iron was deposited on the GaAs surface, prepared by electron beam evaporation from an iron wire. The GaAs substrate was kept at room temperature and was evenly rotated around the azimuth during the evaporation in order to obtain a homogenous Fe film. The subsequently recorded

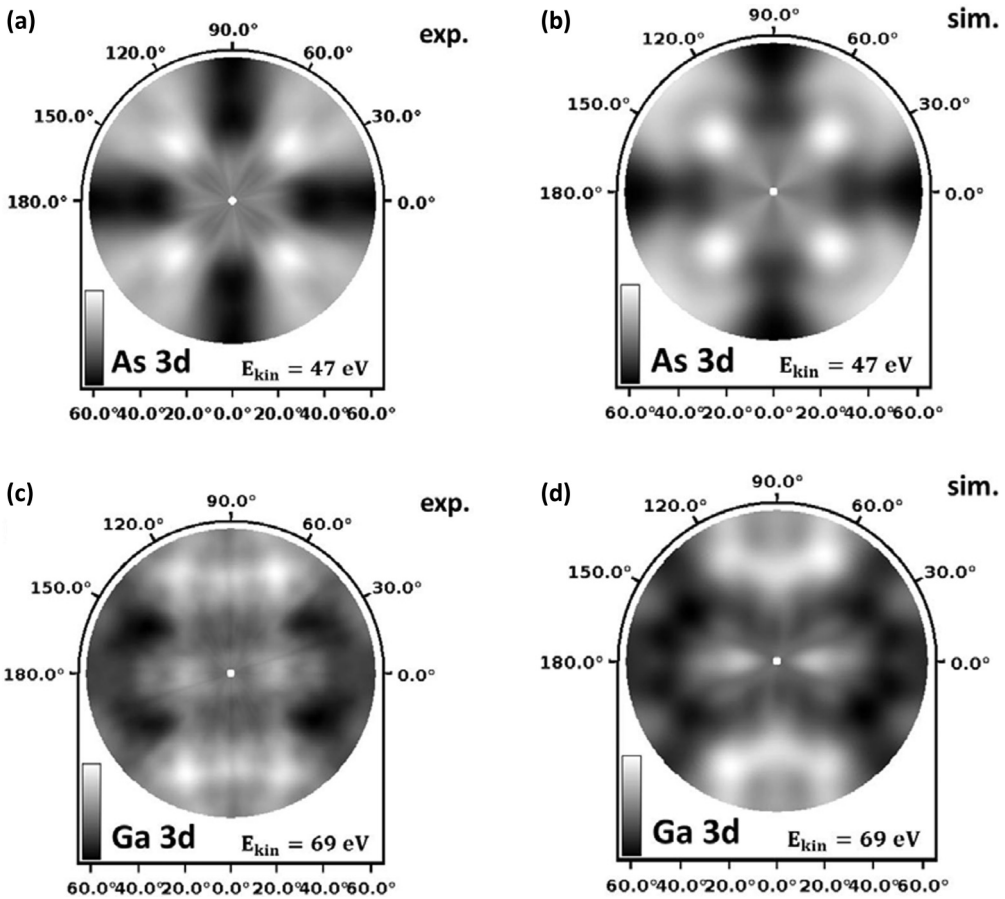

FIG. 3. Experimental XPD patterns of As 3*d* (a) and Ga 3*d* (c) of the (4×2)-reconstructed sample and best simulated XPD patterns of As 3*d* (b) and Ga 3*d* signals (d) for the two-dimer model. The simulated XPD patterns are in excellent agreement with the experimental data.

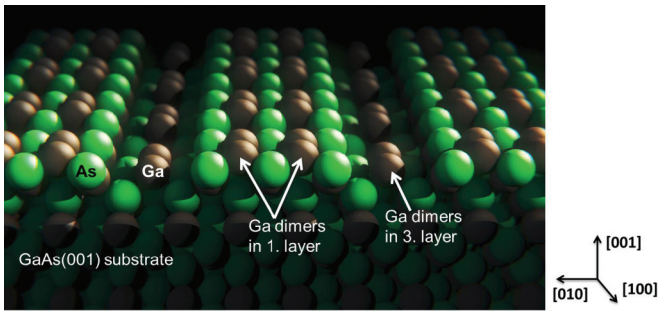

FIG. 4. (Color online) The schematic diagram of the two-dimer model of the GaAs(001)-(4 × 2) reconstruction. Two Ga dimers in the first layer and one Ga dimer in the third layer are denoted. For the fourth layer and below, GaAs is found in a pure zinc-blende structure. The GaAs substrate has a lattice constant of 5.654 Å.

LEED pattern showed a well-ordered (1 × 1) surface of Fe on the GaAs substrate indicating a low defect density. The layer thickness was calculated to be ≈10 Å.[36] This correlates to a ≈0.2 ML/min growth.

In the last step, magnesium oxide was deposited on Fe film by electron beam evaporation from an MgO crystal. During the preparation, MgO was deposited on the Fe/GaAs sample being kept at room temperature. The sample was rotated around the surface normal during MgO evaporation. From the XPD data we calculated a mean layer thickness of ≈4.5 Å.[37] This is equivalent to a growth condition of 0.05 ML/min. During the preparation, each of the layers of the three-layer system MgO/Fe/GaAs was carefully investigated by XPS and XPD.

IV. RESULTS AND DISCUSSION

A. GaAs (4 × 2)-reconstructed substrate

Figures 1 and 2 show core-level spectra of the As 3*d* and Ga 3*d* signals of the clean (4 × 2)-reconstructed surface. The best least-squares fits of the As 3*d* and Ga 3*d* signals resulted in a deconvolution of two and three peaks, respectively. The fitting parameters are summarized in Table I. For the As 3*d* level, component $A1$ increases for increasing polar angles, while the bulk related signal B_{As} is decreasing at the same time.

TABLE II. Parameters of the Gaussian fit for the Fe 3*p* core-level spectra shown in Fig. 5. The intensity ratio of the spin-orbit split $3p_{3/2}$ and $3p_{1/2}$ components was set constant to 2:1.

	E_{kin} (eV)	FWHM (eV)	SOC (eV)
Fe bulk	123.29	0.36	0.80
$F1$	121.99	1.10	0.80
$F2$	118.92	1.10	0.80

The surface state presented by component $A1$ is essential for obtaining an excellent result within the fitting procedure.[39] For the Ga 3*d* signal, the components $G1$ and $G2$ are increasing with respect to the bulk signal B_{Ga} at a polar angle of 60° while the bulk signal decreases. The increase for the component $G1$ is larger than for the component $G2$, as can be seen in Fig. 2. Since the signals $G1$ and $G2$ originate from atoms located at the surface, with $G1$ atoms defining the topmost layer of the surface, their signal rises most for the surface sensitive photoemission geometry at a polar angle of $\theta = 60°$.

Figures 3(a) and 3(b) show the diffraction patterns of the full peak area of As 3*d* and Ga 3*d* signals. As a first interesting experimental finding the XPD pattern of the As 3*d* signal shows a fourfold rotational symmetry, whereas the pattern of the Ga 3*d* signal shows a twofold symmetry. This is surprising since the top three surface layers of GaAs are mostly involved in the (4 × 2) reconstruction,[24] thus both elements are expected showing the same rotational symmetry in their diffraction patterns. The structure of pure GaAs is a zinc blende, with both Ga and As in fcc lattices within GaAs. Therefore, in either way, both patterns are expected to show a twofold rotational symmetry for the (001)-surface orientation. In order to examine this assumption, diffraction patterns of Ga and As in a zinc-blende structure with a lattice constant of $a_{\mathrm{GaAs}} = 5.654$ Å were simulated. The simulations yielded two patterns of twofold rotational symmetry. A comparison between experimental and simulated patterns resulted in *R* factors for As and Ga with $R = 1.14$ and $R = 0.85$, respectively, which indicates rather poor agreement. Assuming that the observed different rotational symmetries in the experimental XPD pattern for the Ga and As signal are a consequence

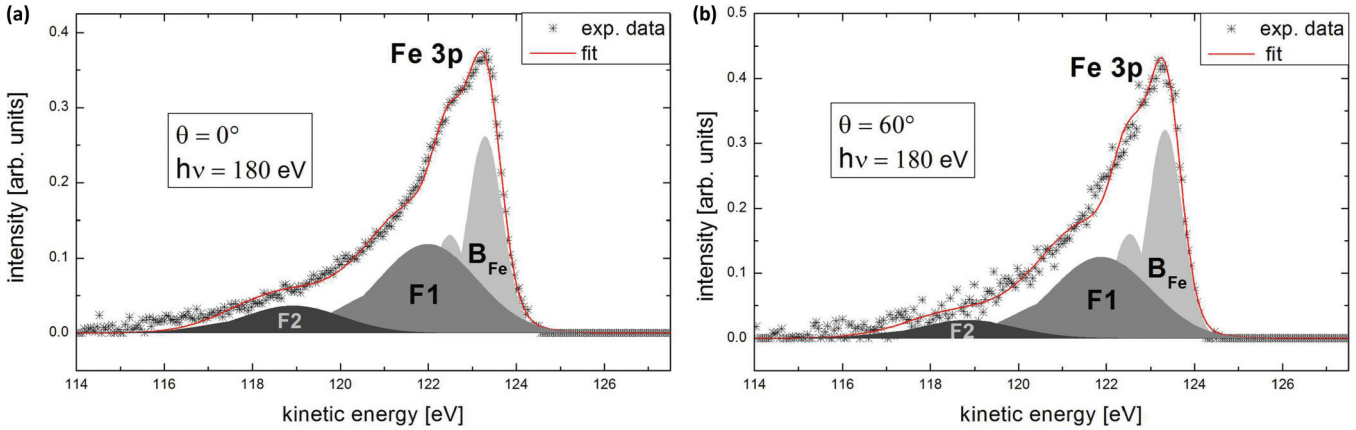

FIG. 5. (Color online) Fe 3*p* core-level spectra at $\theta = 0°$ (a) and at $\theta = 60°$ (b) of the iron film on the reconstructed GaAs sample. The increase of the bulk signal B_{Fe} at the surface sensitive polar angle $\theta = 60°$ with respect to the interfacial components $F1$ and $F2$ is illustrated.

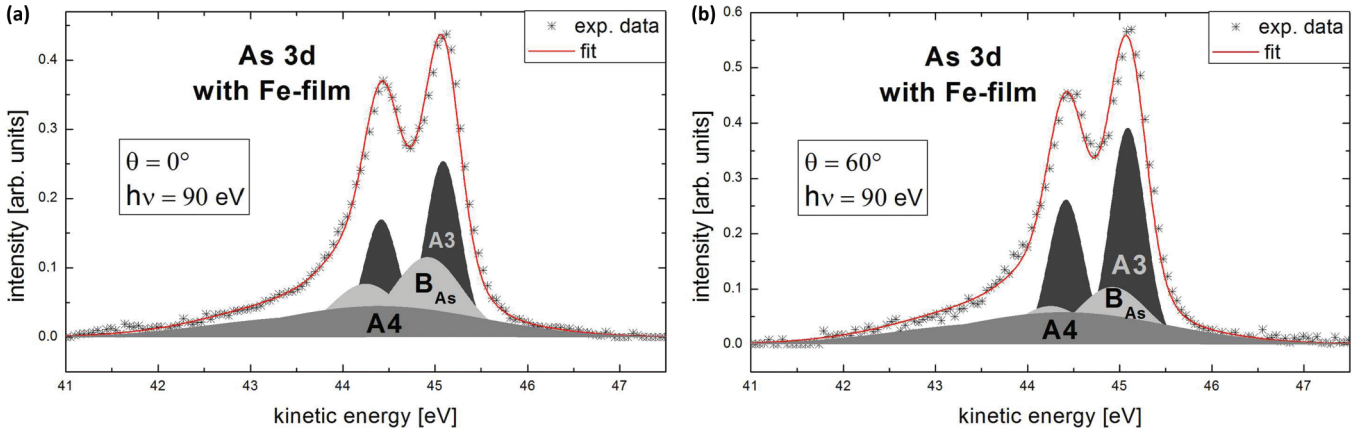

FIG. 6. (Color online) As 3d core-level spectra at $\theta = 0^\circ$ (a) and at $\theta = 60^\circ$ (b) of the GaAs substrate after Fe deposition. The two additional components and the decreasing bulk signal B_{As} at $\theta = 60^\circ$ are shown.

of the (4 × 2)-surface reconstruction we modified the model: Two gallium dimers onto the topmost and one gallium dimer into the third layer of the system were added, as displayed in Fig. 4. This structure, the "two-dimer model" of the (4 × 2) GaAs(001) reconstruction was proposed by Xue *et al.*[24] and Biegelsen *et al.* from STM images.[25] For the modified surface structure, the simulations for the As 3d and Ga 3d signals are in excellent agreement with the experimental data, which is elucidated in Figs. 3(c) and 3(d). When compared to the experimental data the R factors are $R = 0.05$ and $R = 0.10$ for arsenide and gallium, respectively.

The analysis of the GaAs (4 × 2)-reconstructed substrate shows the strong influence of this reconstruction on the As 3d and Ga 3d XPD pattern and confirms the two-dimer model .

B. Fe layer

After deposition of iron onto the reconstructed GaAs high-resolution spectra of the Fe 3p core level were recorded. Figure 5 and Table II present the best results obtained for a curve resolution of the spectra within a fitting procedure. At $\theta = 60^\circ$ the iron substrate signal B_{Fe} is increased with respect to the components $F1$ and $F2$. Further, the components $F1$ and $F2$ corresponding to the Fe^{2+} and Fe^{3+} states are shifted about $\Delta E_{kin} = 1.3$ eV and $\Delta E_{kin} = 4.4$ eV to lower kinetic energies, respectively. Chemically shifted components of the Fe 3p signal were investigated in many cases for iron oxides in the past.[40–43] In this work, the observed energy shifts are not in line with literature[37] as to be related to iron-oxide states of FeO, $Fe2O_3$, or $Fe3O_4$. However, iron is in its second and third oxidation state in a Fe-As[44] and Fe-Ga compound,[45] respectively. Since arsenide and gallium are less electronegative than oxygen this indicates that the components $F1$ and $F2$ result from GaAs substrate atom diffusion into the iron film, or from interface bonding where Ga-Fe and As-Fe are strongly involved. The As 3d and Ga 3d XPS spectra recorded after Fe deposition are shown in Figs. 6 and 7. The results from the Gaussian least-squares fits are listed in Table III. Both spectra show two additional components with respect to the bulk signals, which are shifted about $\Delta E_{kin,A3} = 0.16$ eV, $\Delta E_{kin,A4} = -0.53$ eV, $\Delta E_{kin,G3} = 0.82$ eV, and $\Delta E_{kin,G4} = 1.14$ eV for As 3d and Ga 3d, respectively. The As 3d bulk signal B_{As} decreases for increasing polar angles with respect to the components $A3$ and $A4$. Component $A3$ strongly increases with increasing polar angle and we observe an almost constant component $A4$ of As 3d. Figure 7 shows a strong shift of ≈0.8 eV in the Ga 3d signal and therefore the $G4$ and $G5$ components are found

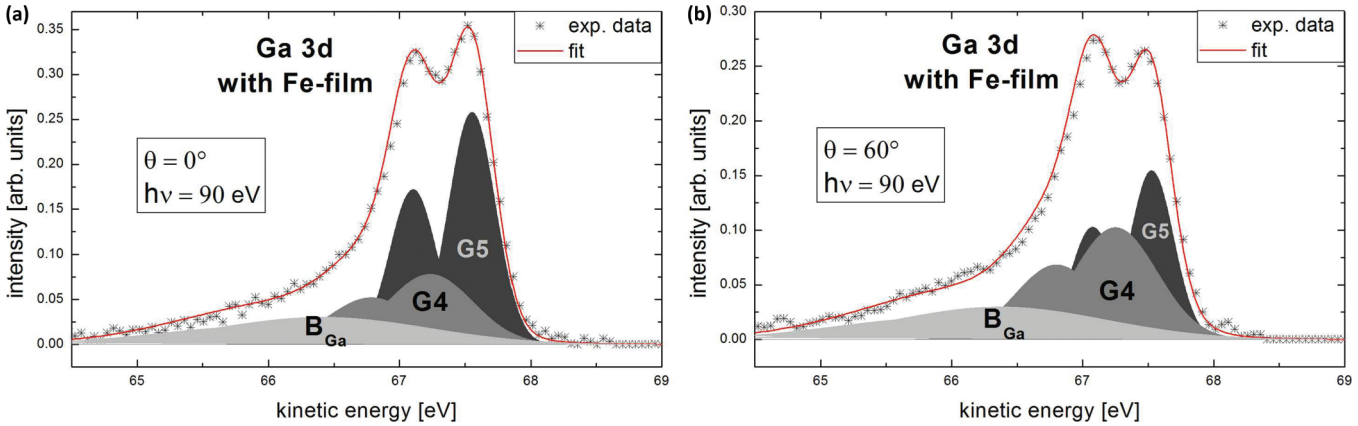

FIG. 7. (Color online) Ga 3d core-level spectra at $\theta = 0^\circ$ (a) and at $\theta = 60^\circ$ (b) of the GaAs substrate after Fe deposited. A strong shift of the complete spectra compared to Fig. 2 is observed.

TABLE III. Parameters of the Gaussian fit for the As 3*d* and Ga 3*d* core-level spectra with an Fe film as shown in Figs. 6 and 7.

	E_{kin} (eV)	FWHM (eV)	SOC (eV)
As bulk	44.92	0.37	0.67
*A*3	45.08	0.18	0.67
*A*4	44.39	1.11	0.67
Ga bulk	66.41	0.80	0.45
*G*4	67,23	0.32	0.45
*G*5	67.55	0.16	0.45

TABLE IV. Parameters of the least-squares fit of the core-level spectra of Fe 3*p* and Mg 2*p* signals of the three-layer system MgO/Fe/GaAs. A Gaussian peak shape is assumed for the signals shown in Fig. 9. The spin-orbit split $2p_{3/2}$ and $2p_{1/2}$ components have a constant intensity ratio of 2:1.

	E_{kin} (eV)	FWHM (eV)	SOC (eV)
*F*3	123.03	0.57	0.8
*F*4	120.85	0.79	0.8
*M*1	125.86	0.50	0.28
*M*2	124.68	0.35	0.28

at nearly the same kinetic energy as the rather small Ga bulk signal B_{Ga}. Component *G*3 decreases while *G*4 increases for rising polar angles. The significant change of the As 3*d* and Ga 3*d* spectra as displayed when comparing Figs. 1 and 2 can be explained by an interface structure consisting of FeAs and FeGa formation. Furthermore, this finding supports the belief that the additional components *F*2 and *F*3 in the Fe 3*p* spectra result from interdiffusion of the GaAs substrate. In the literature Chambers *et al.* and Ruckman *et al.* reported a strong change of the GaAs signals resulting from Fe deposition on a GaAs-(8 × 2) reconstruction[46] and the formation of a Fe/GaAs(110) interface,[23] respectively.

The diffraction pattern of the full peak area of the Fe 3*p* signal shows a fourfold rotational symmetry, as displayed in Fig. 8(a). According to the literature, Fe forms a bcc structure for the here prepared Fe film.[47,48] Within the simulations the bcc structure with a lattice constant of $a_{\mathrm{Fe},bcc} = 2.866$ Å was used as a starting parameter and yielded the very good *R* factor of $R = 0.15$, confirming the crystalline Fe layer at the GaAs surface. During the simulations various structure modifications were performed in order to improve the agreement to the experimental diffraction pattern. The additional components *F*1 and *F*2 in the Fe 3*p* XPS spectra resulting from diffusion of Ga and As may influence the diffraction pattern. Therefore, a Fe/GaAs structure model with a (4 × 2)-reconstructed GaAs substrate was simulated. The reconstruction might be lifted due to the deposition of iron, therefore we simulated the Fe/GaAs system with GaAs being in a zinc-blende structure, too. As a result we found that the structure of the GaAs substrate is of minor importance to the Fe XPD pattern since *R* factors of $R = 1.15$ and worse were obtained in all simulations. This can be explained by an interface which is mostly formed by diffusion, because the crystalline properties of the iron film are dominating the Fe 3*p* XPD pattern. As a further test, a face-centered structure with $a_{\mathrm{Fe},fcc} = 3.647$ Å was assumed for iron within the simulation, leading to a poor accordance with *R* factors larger than $R = 0.45$. Also, a phase transition from bcc to fcc iron films on copper as a function of thickness was discussed in the literature by Kalki *et al.*[49] Therefore, several simulations for fcc and bcc mixed structures were tried, however, no simulations resulted in *R* factors better than $R = 0.68$. The agreement between experimental and simulated patterns was significantly improved by decreasing the vertical distance between the topmost Fe layers of ∼0.1 Å. Figure 8 compares experimental and simulated diffraction patterns with an excellent *R* factor of $R = 0.08$, confirming the crystalline growth of the bcc Fe layer on the GaAs (4 × 2).

C. MgO layer

The Mg 2*p* and Fe 3*p* signals are separated by a few eV only. Figure 9 shows the two signals recorded at $\theta = 0^\circ$ and $\theta = 60^\circ$, together with the result of a peak curve resolution performed for two components in both the magnesium and iron signals. The parameters of the least-squares fits are summarized in Table IV. The magnesium signal shows a strong component M1, which corresponds to the ionized magnesium state Mg^{2+} and an additional component *M*2 corresponding to the magnesium bulk signal. Generally, the Fe 3*p* signal decreases with respect to the Mg 2*p* signal for increasing

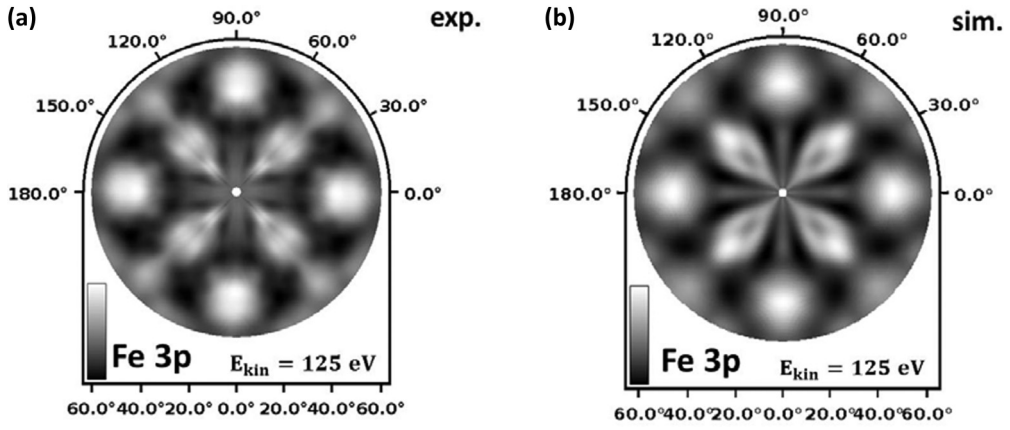

FIG. 8. Experimental XPD pattern of the Fe 3*p* signal (a) and the best simulated pattern obtained for an Fe film in bcc structure (b).

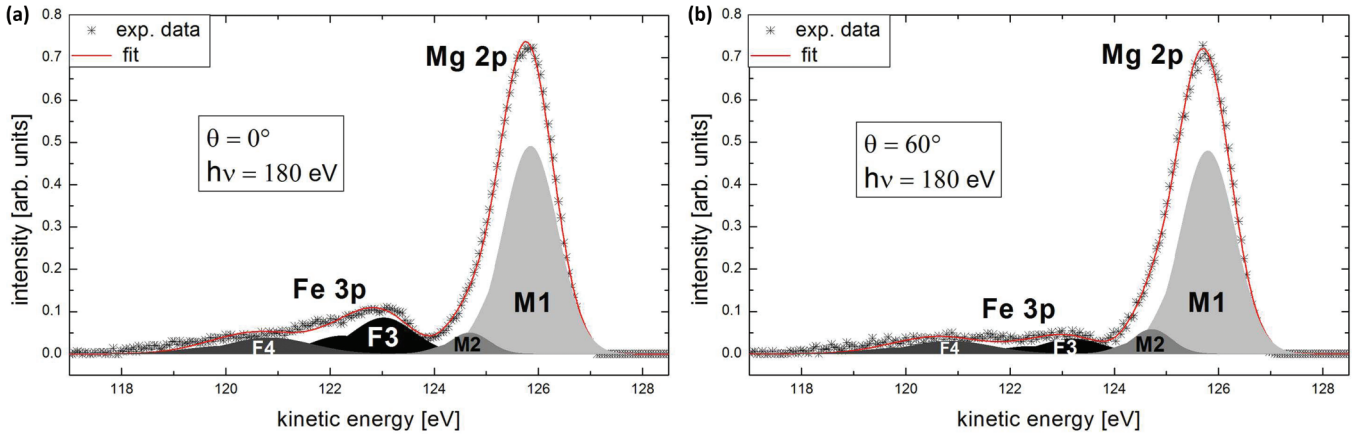

FIG. 9. (Color online) Mg $2p$ and Fe $3p$ core-level spectra at $\theta = 0^\circ$ (a) and $\theta = 60^\circ$ (b) of the three-layer system MgO/Fe/GaAs. The decrease of the Fe $3p$ signal at $\theta = 60^\circ$ clearly shows that MgO is forming the topmost layer of this system.

polar angles, as displayed by the spectrum shown in Fig. 9(b), recorded at $\theta = 60^\circ$. This directly shows that the MgO film is the topmost layer at the surface. The iron component $F3$ of the Fe $3p$ signal corresponds to the iron bulk signal since it is strongly decreasing for increasing polar angles. Finally, the component $F4$ being shifted about $\Delta E_{kin} = 2.18$ eV to lower kinetic energies with respect to the iron bulk signal displays only a rather weak dependence of the peak intensity as a function of polar angle. This additional component is a hint of a possible oxidation of the iron film at the interface resulting from oxygen diffusion due to MgO deposition. The almost constant behavior of component $F4$ with regard to increasing polar angles can be explained by a partial segregation of oxidized Fe due to the MgO mean layer thickness of 4.5 Å.

For analyzing the XPD pattern of the MgO absorbate the experimental data had to be truncated to the Mg signal, because of the previously mentioned overlap of the Fe $3p$ and Mg $2p$ signals. Figure 10(a) displays a fourfold rotational symmetry in the diffraction pattern of the Mg $2p$ signal. In a first simulation, MgO is assumed in a traditional halite structure with a lattice constant of $a_{\mathrm{MgO}} = 4.213$ Å leading to a rather large R factor of $R = 1.14$ indicating bad agreement between the experimental and calculated data. As an important result from this first test, the strongest intensities are displayed being rotated by 45° with respect to the experimental data. This epitaxial relationship between the Fe(001) and MgO(001) surfaces rotation was first reported by Kanaji *et al.*[50] and it was confirmed by further investigations from Vassent *et al.*[51] Therefore, the structure model was modified by a 45° rotation of the topmost MgO layer with respect to a bcc iron elementary cell. As a result, experimental and simulated patterns showed very good agreement. Although the experimental data are truncated, the influence of the iron layer is still existing since the components $F3$ and $M1$ overlap, because they are Gaussian in energy, as can be seen in Fig. 9. Since the XPS spectra indicate an oxidation of Fe, as displayed in Fig. 9, the structure model was modified by adding an FeO layer between bcc Fe and halite MgO, as schematically shown in Fig. 11. Indeed, from the data reported here a system with two FeO layers strongly improves the agreement of the XPD pattern. The interface oxygen atoms between Fe and Mg are shifted towards the MgO film, whereas the oxygen atoms of the layer below are centered within the Fe bcc cell. An

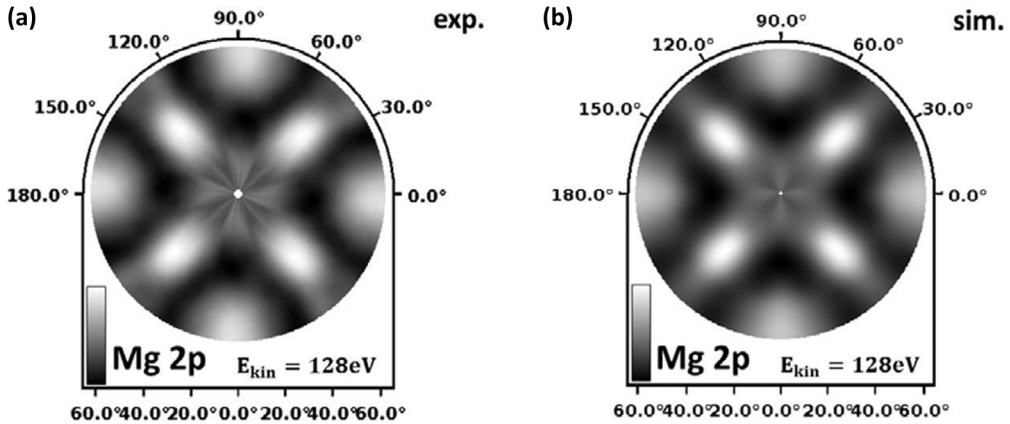

FIG. 10. Experimental XPD pattern of the Mg $2p$ signal (a) and best simulated pattern obtained for a structure with a reduced number of magnesium atoms in the interface as discussed in the text (b). The experimental XPD pattern and the simulated pattern are in excellent agreement.

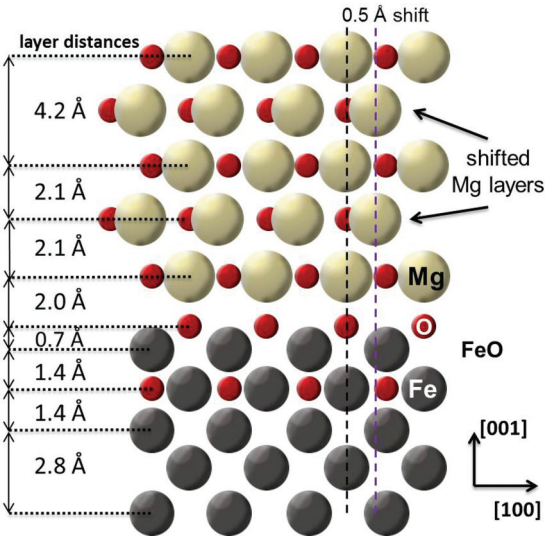

FIG. 11. (Color online) Illustration of the MgO/Fe structure model with two FeO layers in the interface and partially shifted Mg layers as explained in the text. Some of the Mg layers are shifted by 0.5 Å, as indicated. The complete MgO adsorbate film is rotated by 45° with respect to the Fe bcc elementary cell.

oxidized interface consisting of one FeO layer between an Fe substrate and a MgO film was proposed by Meyerheim *et al.*[52] and Yu *et al.*[53] In our work, more than two FeO layers deteriorate the accordance between the experimental and simulated patterns significantly. In a final step, using the genetic algorithm, the magnesium interlayer distance was varied along the [100] direction. The best agreement was achieved for a model where every second Mg layer is slightly shifted, as shown in Fig. 11. The very low R factor of $R = 0.04$ indicates an excellent agreement between the experimental and simulated diffraction patterns, as displayed in Fig. 10.

V. CONCLUSION

In this study, we report on the crystalline properties of the GaAs reconstructed substrate, the Fe film, the MgO film, and the interfaces of the three-layer system MgO/Fe/GaAs. Core-level spectra of As 3*d* and Ga 3*d* prove a successful preparation of the gallium-rich (4×2) reconstruction. The As and Ga diffraction patterns show the strong influence of the GaAs surface reconstruction. For this reconstruction we verify two Ga dimers being located on top of the surface and one dimer located in the third layer. A crystalline bcc structure of iron grown on the GaAs (4×2) surface is indicated by the Fe $3p$ XPD pattern of the Fe $3p$ signal. However, the XPS spectra and XPD pattern indicate an Fe/GaAs interface with a structure principally formed by diffusion. A strong Mg^{2+} state is displayed in the high-resolution spectra of the Mg $2p$ signal. From the diffraction pattern we propose a crystalline interface structure with FeO in the MgO/Fe interface and partially shifted Mg layers in the MgO topmost layer.

The interesting finding of the shifted Mg layers requires further measurements in order to identify the physical meaning of these shifted Mg atoms. A speculative explanation for the observed shifted Mg atoms is the huge difference in Fe and MgO lattice constants which are $a_{Fe} = 2.866$ Å and $a_{MgO} = 4.213$ Å, respectively. Therefore, a measurement of atoms within the film is necessary. Another explanation could be the strong dependence of the MgO film on its preparation procedure, as reported for LEED and electron energy loss spectroscopy by Xue and Guo.[54]

ACKNOWLEDGMENTS

We gratefully acknowledge useful discussions with A. Herdt, D. Gottlob, and H. Krull and thank the DELTA staff for continuous support during beamtimes. This work was supported by the Land Nordrhein-Westfalen, the NRW Forschungsschule, and the Bundesministerium für Bildung und Forschung.

*dominique.handschak@tu-dortmund.de

[1] M. Jullière, Phys. Lett. A **54**, 225 (1975).
[2] L.-N. Tong, F. Matthes, M. Müller, C. M. Schneider, and C.-G. Lee, Phys. Rev. B **77**, 064421 (2008).
[3] M. S. Xue, W. Li, F. J. Wang, J. P. Yao, and J. S. Lu, Vacuum **85**, 550 (2010).
[4] S. Parkin, C. Kaiser, A. Panchula, P. Rice, B. Hughes, M. Samant, and S. Yang, Nat. Mater. **3**, 862 (2004).
[5] W. H. Butler, X.-G. Zhang, T. C. Schulthess, and J. M. MacLaren, Phys. Rev. B **63**, 054416 (2001).
[6] S.-H. Yang, B. Balke, C. Papp, S. Döring, U. Berges, L. Plucinski, C. Westphal, C. M. Schneider, S. S. P. Parkin, and C. S. Fadley, Phys. Rev. B **84**, 184410 (2011).
[7] G. Autès, J. Mathon, and A. Umerski, Phys. Rev. B **82**, 115212 (2010).
[8] B. Kardasz, E. A. Montoya, C. Eyrich, E. Girt, and B. Heinrich, J. Appl. Phys. **109**, 3 (2011).
[9] G. Binasch, P. Grünberg, F. Saurenbach, and W. Zinn, Phys. Rev. B **39**, 4828 (1989).
[10] M. N. Baibich, J. M. Broto, A. Fert, F. Nguyen Van Dau, F. Petroff, P. Etienne, G. Creuzet, A. Friederich, and J. Chazelas, Phys. Rev. Lett. **61**, 2472 (1988).
[11] D. Hägele, M. Oestreich, W. Rühle, N. Nestle, and K. Eberl, Appl. Phys. Lett. **73**, 3 (1998).
[12] H. J. Zhu, M. Ramsteiner, H. Kostial, M. Wassermeier, H.-P. Schönherr, and K. H. Ploog, Phys. Rev. Lett. **87**, 016601 (2001).
[13] E. I. Rashba, Phys. Rev. B **62**, R16267 (2000).
[14] G. X. Du, S. G. Wang, Q. L. Ma, Y. Wang, R. C. C. Ward, X.-G. Zhang, C. Wang, A. Kohn, and X. F. Han, Phys. Rev. B **81**, 064438 (2010).
[15] F. Bonell, S. Andrieu, A. M. Bataille, C. Tiusan, and G. Lengaigne, Phys. Rev. B **79**, 224405 (2009).
[16] Y. B. Xu, E. T. M. Kernohan, D. J. Freeland, A. Ercole, M. Tselepi, and J. A. C. Bland, Phys. Rev. B **58**, 890 (1998).
[17] C. Raisch, T. Chassé, C. Langheinrich, and A. Chassé, J. Appl. Phys. **112**, 9 (2012).
[18] F. R. Negreiros, E. A. Soares, A. de Siervo, R. Paniago, V. E. de Carvalho, and R. Landers, Phys. Rev. B **81**, 085437 (2010).

[19]A. de Siervo, E. A. Soares, R. Landers, and G. G. Kleiman, Phys. Rev. B **71**, 115417 (2005).
[20]T. T. Tran, S. Thevuthasan, Y. J. Kim, G. S. Herman, D. J. Friedman, and C. S. Fadley, Phys. Rev. B **45**, 12106 (1992).
[21]R. Moosbühler, F. Bensch, M. Dumm, and G. Bayreuther, J. Appl. Phys. **91**, 3 (2002).
[22]J.-M. Lee, S.-J. Oh, K. J. Kim, S.-U. Yang, J.-H. Kim, and J.-S. Kim, Phys. Rev. B **75**, 125421 (2007).
[23]M. W. Ruckman, J. J. Joyce, and J. H. Weaver, Phys. Rev. B **33**, 7029 (1986).
[24]Q.-K. Xue, T. Hashizume, and T. Sakurai, Prog. Surf. Sci. **56**, 1 (1997).
[25]D. K. Biegelsen, R. D. Bringans, J. E. Northrup, and L.-E. Swartz, Phys. Rev. B **41**, 5701 (1990).
[26]E. Moreau, S. Godey, F. J. Ferrer, D. Vignaud, X. Wallart, J. Avila, M. C. Asensio, F. Bournel, and J.-J. Gallet, Appl. Phys. Lett. **97**, 3 (2010).
[27]Y.-J. Chang, C. L. Munsee, G. S. Herman, J. F. Wager, P. Mugdur, D.-H. Lee, and C.-H. Chang, Surf. Interface Anal. **37**, 398 (2005).
[28]D. A. Shirley, Phys. Rev. B **5**, 4709 (1972).
[29]A. Liebsch, Phys. Rev. Lett. **32**, 1203 (1974).
[30]K.-M. Schindler, V. Fritzsche, M. C. Asensio, P. Gardner, D. E. Ricken, A. W. Robinson, A. M. Bradshaw, D. P. Woodruff, J. C. Conesa, and A. R. González-Elipe, Phys. Rev. B **46**, 4836 (1992).
[31]L.-Q. Wang, A. E. Schach von Wittenau, Z. G. Ji, L. S. Wang, Z. Q. Huang, and D. A. Shirley, Phys. Rev. B **44**, 1292 (1991).
[32]R. Gunnella, F. Solal, D. Sebilleau, and C. Natoli, Comput. Phys. Commun. **132**, 251 (2000).
[33]D. Sébilleau, R. Gunnella, Z.-Y. Wu, S. Di Matteo, and C. Natoli, J. Phys.: Condens. Matter **18**, R175 (2006).
[34]D. P. Woodruff and A. M. Bradshaw, Rep. Prog. Phys. **57**, 1029 (1994).
[35]R. Döll and M. V. Hove, Surf. Sci. **355**, L393 (1996).
[36]D. Briggs and M. Seah, *Practical Surface Analysis* (Wiley, Chichester, 1990), Vol. 1.
[37]J. Moulder, *Handbook of X-Ray Spectroscopy* (Perkin-Elmer Co., Minnesota, 1978).
[38]E. Bullock, R. Gunnella, C. Natoli, H. Yeom, S. Kono, L. Patthey, R. Uhrberg, and L. Johansson, Surf. Sci. **352–354**, 352 (1996).
[39]G. Le Lay, D. Mao, A. Kahn, Y. Hwu, and G. Margaritondo, Phys. Rev. B **43**, 14301 (1991).
[40]V. Castro, G. Polzonetti, S. Ciampi, G. Contini, and O. Sakho, Surf. Sci. **293**, 41 (1993).
[41]F. Parmigiani and L. Sangaletti, J. Electron Spectrosc. Relat. Phenom. **98–99**, 287 (1999).
[42]B. Handke, J. Simonsen, M. Bech, Z. Li, and P. Møller, Surf. Sci. **600**, 5123 (2006).
[43]N. S. McIntyre and D. G. Zetaruk, Anal. Chem. **49**, 1521 (1977).
[44]S. Hilpert and T. Dieckmann, Berichte der deutschen chemischen Gesellschaft **44**, 2378 (1911).
[45]B. Predel and W. Vogelbein, Thermochim. Acta **13**, 133 (1975).
[46]S. A. Chambers, F. Xu, H. W. Chen, I. M. Vitomirov, S. B. Anderson, and J. H. Weaver, Phys. Rev. B **34**, 6605 (1986).
[47]G. A. Prinz and J. J. Krebs, Appl. Phys. Lett. **39** (1981).
[48]J. J. Krebs, B. T. Jonker, and G. A. A. Prinz, Appl. Phys. Lett. **61**, 4 (1987).
[49]K. Kalki, D. D. Chambliss, K. E. Johnson, R. J. Wilson, and S. Chiang, Phys. Rev. B **48**, 18344 (1993).
[50]T. Kanaji, K. Asano, and S. Nagata, Vacuum **23**, 55 (1973).
[51]J. L. Vassent, M. Dynna, A. Marty, B. Gilles, and G. Patrat, J. Appl. Phys. **80**, 9 (1996).
[52]H. L. Meyerheim, R. Popescu, J. Kirschner, N. Jedrecy, M. Sauvage-Simkin, B. Heinrich, and R. Pinchaux, Phys. Rev. Lett. **87**, 076102 (2001).
[53]B. D. Yu and J.-S. Kim, Phys. Rev. B **73**, 125408 (2006).
[54]M. Xue and Q. Guo, J. Chem. Phys. **127**, 5 (2007).